Chapter 3

Microwave-assisted rapid synthesis and molecular weight of Polyethyleneimine-dependent selective surface interaction and antimicrobial activity of functional silver nanoparticles

3.1 Introduction

The technologies for introducing a cationic charge on inorganic materials (including nanoparticles) typically involve surface grafting with amine groups and coating with cationic polymers (e.g., Polyethyleneimine (PEI), poly-amidoamine, and poly-lysine) through either covalent or electrostatic association (Radu et al., 2004; Bharali et al., 2005; Xia et al., 2009). PEIs are synthetic cationic polymers that compact DNA and siRNA into complexes, which are taken up in cells (Xia et al., 2009). Since the cytotoxicity of PEI coating can interfere with the efficacy of the delivery system, by selecting optimal polymeric lengths to control transfusion efficiency, one may simultaneously reduce or eliminate the toxic effects of cationic polymer-coated nanoparticles. In turn, this directed us to investigate the synthesis and coating of silver nanoparticles (AgNPs) by PEI as a function of polymeric molecular weight (M_W) (Burda et al., 2005; Morones et al., 2005) We are interested in the interaction of PEI-coated Ag-NPs with multidrug-resistant (MDR) microbes (Morones et al., 2005 Rodzig et al., 2013; Franci et al., 2015; Rai et al., 2009). Silver is considered a Lewis acid that tends to react with a Lewis base; Lewis bases include phosphorous and sulfur-containing biomolecules, the significant components of the cell membrane, proteins, and DNA bases (Wiley et al., 2005). Hence, Ag-NPs can accumulate on the cell membrane and cause morphological changes such as shrinkage of the cytoplasm, membrane detachment, and the formation of numerous electron-dense pits,

disrupting the cell membrane (Dakal et al., 2016). A cationic polymer coating may allow for the selective transfusion of silver nanoparticles.

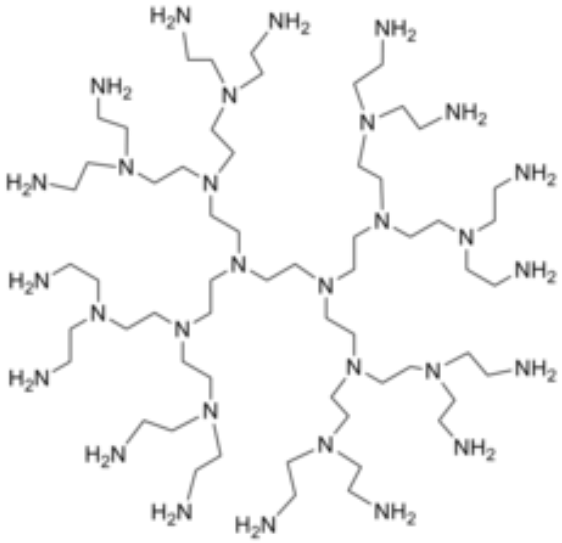

Scheme 3.1 Chemical structure of branched polyethyleneimine.

We have already demonstrated that PEI, along with an organic reducing agent, allows for controlled synthesis of gold nanoparticles (Pandey et al., 2017). Since the amine functionality of cationic polymer enables microwave activity, it is desirable to control the reduction of the noble metal cation under microwave incubation. Interestingly, we have observed rapid synthesis of PEI-coated silver nanoparticles within less than 1 minute under microwave incubation. In addition, nanoparticle formation may further be controlled as a function of MW of the synthetic polymer. The antimicrobial activity of the nanoparticles was examined using *A. baumannii*, which is the predominant cause of hospital-acquired infections in intensive care unit-admitted patients; clinical manifestations of infection include pneumonia, bacteremia, wound infections, and urinary tract infections. The antimicrobial activity of several new types of nanomaterials has recently been demonstrated. For example, Matharu et al. demonstrated the antimicrobial activity of tungsten nanoparticles and tungsten nanocomposite fibers against bacteriophage T4, *Escherichia coli*, and *Staphylococcus aureus* (Matharu et al., 2020) the antimicrobial activity of graphene nanoparticles was also recently demonstrated (Matharu et

al., 2018). One recent study demonstrated that fluorescence imaging could be used to understand protein–nanoparticle interactions (Shi et al., 2019). Silver nanoparticles with cationic polymers may either alter the intrinsic fluorescence of surface-active proteins or maintain high transfusion efficiency across the bacterial cell membrane; the fluorescence behavior of cytoplasmic fluorescent biomolecules may provide insight into this process. The wide variation in PEI MW between 1300 and 75,000 may allow for the selective transfusion of PEI-coated Ag-NPs across the bacterial cell membrane. Indeed, valuable information on the impact of cationic polymeric M_W on antimicrobial activity may be obtained. The antibacterial activity of the AgNPs, as detected by fluorescence imaging, may be attributed to surface binding properties, active biomolecule/ion release, and generation of high oxidative stress as a function of the polymeric coating on the silver nanoparticles (Matsumura et al., 2003). This study used fluorescence imaging of PEI-coated AgNPs with three different MWs to understand nanoparticle–*A. baumannii* cell membrane interactions, specifically antimicrobial activity, are a function of PEI's molecular weight.

3.2 Experimental

3.2.1 Materials

All MW PEI, silver nitrate ($AgNO_3$), fluorescein, and bovine serum albumin were obtained from Sigma Aldrich (Bangalore, Karnataka, India). Bacterial culture media such as Muller Hinton Broth (MHB), Muller Hinton Agar (MHA), and Nutrient Broth (NB) were purchased from Hi-Media Laboratories Ltd. (Mumbai, Maharashtra, India). Plastic ware was purchased from Tarsons Product Pvt. Ltd. (Kolkata, West Bengal, India). The antibiotics and other routine chemicals were purchased from Sigma Aldrich (St. Louis, MO, USA). The organic solvents were purchased from Merck Life Science Private Limited (Bangalore, Karnataka, India). All of the reagents were analytical grade.

3.2.2 Bacterial strain

We have isolated one strain of *A. baumannii* from the endotracheal tube secretions of one ICU-admitted male patient who developed ventilator-associated pneumonia. This strain was identified based on the culture characteristics of MacConkey agar, blood agar, and Gram stain. Biochemical tests included catalase, oxidase, sugar fermentation test, and citrate utilization test. On antibiotic susceptibility testing, this strain was only sensitive to polymyxin B; it showed resistance to the other tested antibiotics, which include amoxicillin-clavulanic acid, ceftazidime, gentamycin, amikacin, ciprofloxacin, levofloxacin, ampicillin-sulbactam, piperacillin-tazobactam, and the carbapenem group of antibiotics.

3.2.3 Synthesis of PEI-functionalized silver nanoparticles

3.2.4 PEI-1 (M_W 750,000 Da) and cyclohexanone-mediated synthesis of AgNP-1

Ethylene glycol (120 µL) and a methanolic solution of 1-vinyl 2-pyrrolidone (50 µL of a 250 mM solution) were placed in 2 mL glass vial, followed by the addition of a methanolic solution of $AgNO_3$ (10 µL of a 10 mM solution), PEI (150 µL of a 4mg/ mL solution), and cyclohexanone (20 µL). The reaction mixture was thoroughly mixed on a vortex mixer for 30 seconds and placed in a microwave oven for 15 seconds. The cycle was repeated four to six times in the microwave oven, resulting in the appearance of a deep yellow color that indicated the formation of AgNP-1.

3.2.5 PEI-2 (M_W 1300 Da) and formaldehyde-mediated synthesis of AgNP-2

Ethylene glycol (120 µL) and a methanolic solution of 1-vinyl 2-pyrrolidone (50 µL of a 25 mM solution) were placed in a 2 mL glass vial, followed by the addition of a methanolic solution of $AgNO_3$ (10 µL of a 10 mM solution), PEI (20 µL of a 6.25 mg/mL solution), and formaldehyde (10 µL). The reaction mixture was thoroughly mixed on a vortex mixer for 30 seconds and placed in a microwave oven for 15 seconds. The cycle was repeated two to five times in a microwave oven, resulting in the appearance of a deep yellow color that indicated the formation of AgNP-2.

3.2.6 PEI-3 (MW 60,000 Da) and cyclohexanone-mediated synthesis of AgNP-3

Ethylene glycol (120 µL) and a methanolic solution of 1-vinyl 2-pyrrolidone (50 µL of a 50 mM solution) were placed in 2 mL glass vial, followed by the addition of a methanolic solution of $AgNO_3$ (10 µL of a 10 mM solution), PEI-3 (16.4 mg/mL; 100 µL), and cyclohexanone (20 µL). The reaction mixture was thoroughly mixed on a vortex mixer for 30 seconds and placed in a microwave oven for 15 seconds. The cycle was repeated two to three times in a microwave oven, resulting in the appearance of a deep brown color that indicated the formation of Ag-NP-3.

3.2.7 Synthesis of PEI-mediated Ag-Au bimetallic Nanoparticles

All three (MW. Dependent of PEI) bimetallic nanoparticles were synthesized simultaneously by mixing a methanolic suspension of HAuCl4 (50µl; 25 mM) with the prepared suspension of silver nanoparticles synthesis system followed by the vortex mixing for 30 sec. and incubated in microwave oven for 15-sec pulse (3-4 times).

3.2.8 Characterization of functionalized Ag-NPs

All AgNPs were characterized using a U-2900 UV-Vis spectrometer (Hitachi, Tokyo, Japan) over the 250–800 nm scan range. Transmission electron microscopy and electron diffraction (SAED) analysis of AgNPs was carried out using a Tecnai G2 20 Twin instrument (FEI, Hillsboro, OR, USA) at the IIT (BHU) Central Instrumentation Facility. Samples were prepared by diluting the AgNPs in methanol and drop-casting the solution on carbon-coated copper grids of 300 mesh. Zeta potential analysis was performed using a Zetasizer instrument (Malvern Panalytical, Malvern, UK).

3.2.9 Assessment of antibacterial activity and MIC and MBC determinations of AgNPs

The silver nanoparticles were evaluated for their activity against *A. baumannii* using the 2-fold serial dilution method. The MIC and MBC values of synthesized AgNPs against *A. baumannii*

were determined using the broth microdilution in a flat bottom sterile 96-well microtiter plate. In short, an overnight grown culture of *A. baumannii* in MHB medium was centrifuged; the obtained pellet was suspended in fresh MHB medium for 4 h to achieve log phase at 37 °C. A 0.5 MacFarland bacterial suspension containing 0.5×10^8 cfu/mL was prepared for further downstream processing. A working suspension of 112 µg/mL for each type of Ag-NP was prepared; 100 µL of each suspension was distributed in each well using the double dilution approach; the final concentration was between 0.43 and 112 µg/mL. Subsequently, 100 µL of 0.5 MacFarland bacterial suspension was added in each well. Polymyxin B was used as a positive control; no AgNPs were placed in the test control. The microtiter plate was incubated at 37 °C for 24 h; a visual demonstration of complete bacterial inhibition (i.e., a visually clear well) was recorded as the MIC. Subsequently, a 5 µL suspension from the plate was sub-cultured on the MHA plates for 24 h; bacterial growth on the plate was subsequently observed. The MBC was determined as the concentration of AgNPs for which no growth was observed on sub-cultured plates.

3.2.10 Fluorescence spectroscopic studies

All the fluorescence (2D and 3D) spectroscopic studies were conducted on an F-7000 fluorescence spectrophotometer (Hitachi, Tokyo, Japan) in ultra-purified water.

3.2.11 Determination of dynamic quenching of fluorophore fluorescein by PEI-capped AgNPs

An aqueous solution of fluorescein (10 µM) was prepared; emission spectra at an excitation wavelength of 450 nm (EEM 450–510 nm for 3D spectra) were recorded, followed by the addition of an aqueous suspension of PEI-capped Ag-NPs (20 µL of 5 µg/mL solution). In the same suspension, 10^4 cells of *A. baumannii* (log-phase cells, washed two times with sterile purified water) were added and incubated for 10 min; 2D and 3D spectra were subsequently

recorded. 10^8 cells/mL were subsequently added to the same suspension; the emission spectra were recorded.

3.2.12 Cell surface-expressed protein–Ag-NP interaction and membrane fracture studies

A log-phase culture grown in a nutrient broth of *A. baumannii* was centrifuged at 8000 rpm for 6 min; it was then washed two to three times with sterile purified water and adjusted to a concentration of 10^4 cells/mL in water. Intrinsic fluorescence spectra of the surface-expressed proteins were recorded using excitation/emission matrix spectroscopy at 280 and 300 nm. All of the as-prepared AgNPs were incubated with 10^4 cells/mL. MICs were recorded for 1 or 3 h in three tubes; fluorescence spectra were obtained using 2D and 3D EEM. Data were obtained using bovine serum albumin (2 μg/mL) in the same manner as cells. All PEI-functionalized AgNPs were incubated at the corresponding MBC with 10^6 cells/mL for 6 h at room temperature. After 6 h, the cell suspensions were centrifuged at 10,000 rpm for 6 min. The supernatant was collected; 2D fluorescence spectra were recorded separately using EEM at 280 and 300 nm.

3.3 Results & Discussion

3.3.1 Microwave-assisted, Polyethyleneimine-mediated synthesis of silver nanoparticles

The PEI-capped silver cation gets reduced under microwave irradiation in the presence of an organic reducing agent, namely cyclohexanone or formaldehyde, and allows for the formation of three different silver nanoparticles depending on the size and zeta potential. Figure 3.1(A) shows the UV-Vis absorbance spectrum of the produced silver nanoparticles coated with PEI of three different M_{W}s, such as AgNP-1, AgNP-2, and AgNP-3. Figure 3.1 (A, i) shows the results recorded from AgNP-1, Figure 3.1(A, ii) shows the results recorded from AgNP-2, and Figure 3.1(A, iii) shows the results recorded from AgNP-3. The process allowed for the rapid formation of AgNPs regardless of M_W. The properties of AgNP-1, AgNP-2, and AgNP-3 differed as a function of M_W. Further, the concentration of PEI also affected the physico-

chemical properties of AgNPs. The AgNPs were characterized by transmission electron microscopy (TEM) (Figure 3.1(B)) and by zeta potential measurements (Figure 3.1(C)) (Table 3.1).

3.3.2 Bactericidal activity, minimum inhibitory concentration, and minimum bactericidal concentration of AgNPs

The three AgNPs showed bactericidal activity against *A. baumannii*; a variation in bactericidal activity was noted based on M_W (Figure 3.2 (a)). The minimum inhibitory concentration (MIC) and minimum bactericidal concentration (MBC) values of each silver nanoparticle (AgNPs) were determined by the broth microdilution method in flat-bottom sterile microtiter plates. The MBC values for AgNP-1, AgNP-2, and AgNP-3 against the strain of *A. baumannii* were 5, 10, and 5 μg/mL, respectively. The MBC values for AgNP-1, AgNP2, and AgNP-3 were 10, 20, and 10 μg/mL, respectively (Figure 3.2(b)). It was observed that the antibacterial activity of Ag-NPs depends on the M_W of PEI (Figure 3.2). Furthermore, it was observed that AgNPs capped with high-molecular-weight PEI had more potent bactericidal activity than AgNPs capped with low-molecular-weight PEI. The differential bactericidal activity may be attributed to the differences in the branching of PEI among the samples; the highly branched PEI (M_W 750,000 Da)-capped AgNPs (AgNP-1) and moderate branched PEI (M_W 60,000 Da)-capped AgNPs (AgNP-3) showed lower MIC values than unbranched PEI (M_W 1300 Da)-capped AgNPs (AgNP-2). As such, it appears that branched PEI interacts more stably with the outer membrane of *A. baumannii*, which in turn destabilizes the bacterial cell membrane.

Table 3.1 Physico-chemical property of as prepared PEI stabilized silver nanoparticles and respective MIC & MBCs against *A. baumminii*.

Prepared AgNPs	PEI molecular weight	Absorbance Maxima (nm)	Shape/Size (nm)	Zeta potential (mV)	Crystal symmetry	MIC/MBC μg/mL

AgNP-1	750 kDa.	405	Spherical/ 22.0	30	FCC	5/10
AgNP-2	1.3 kDa.	415	Spherical/ 4.5	18	FCC	10/20
AgNP-3	60 kDa.	408	Spherical/ 2.6	32	FCC	5/10

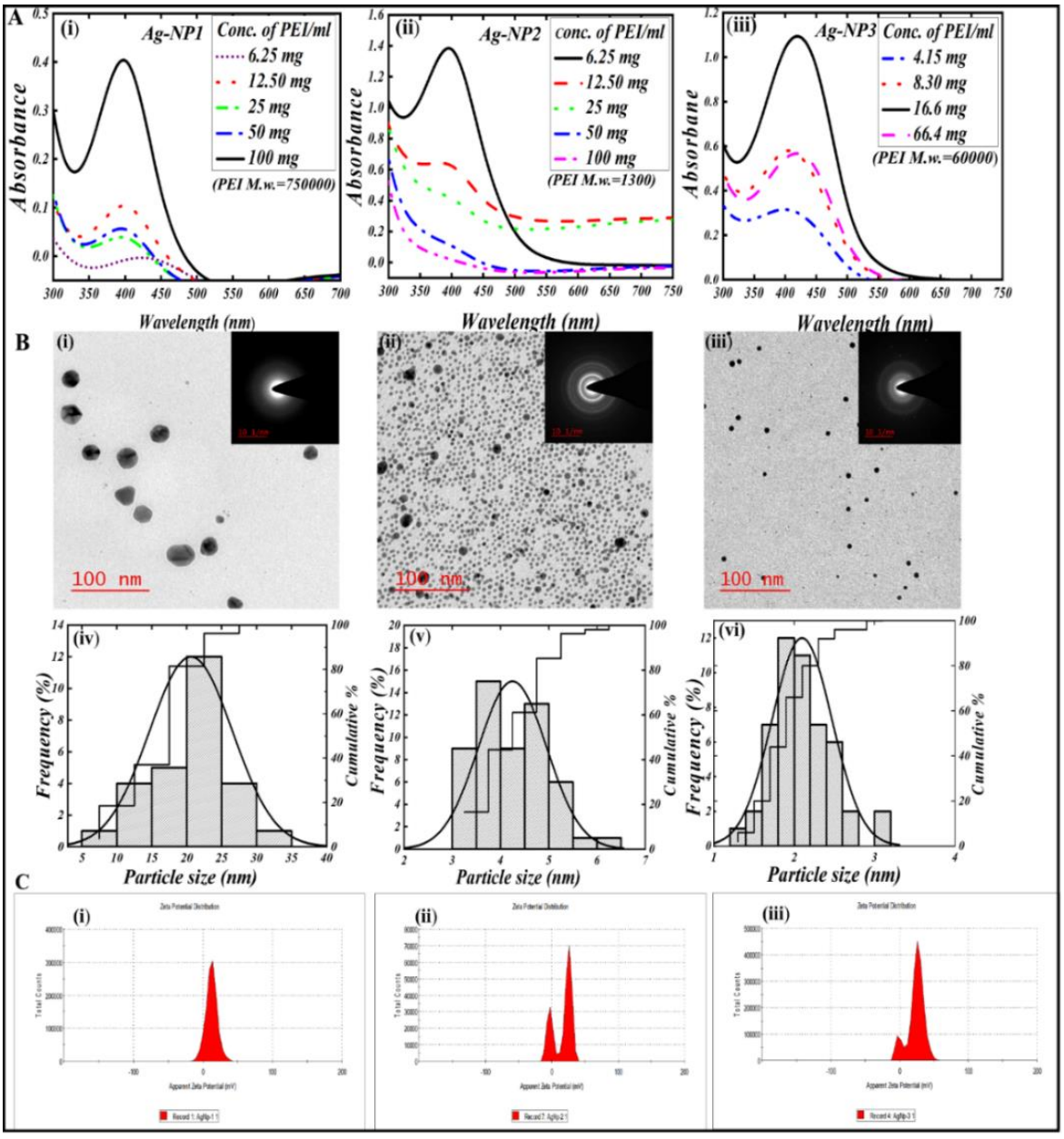

Figure 3.1 (A) Representing the characterization of Synthesised AgNPs by UV-Vis Spectrophotometry, AgNP-1 (i), AgNP-2 (ii) and AgNP-3 (iii); (B) Showing the characterization result of synthesized as AgNPs by TEM imaging with their SAED pattern (inset) and size distribution plot; AgNP-1 (i, iv), AgNP-2 (ii, v) and AgNP-3(iii, vi); (C) Representing the Zeta potential analysis of AgNPs. AgNP-1 (i), AgNP-2 (ii) and AgNP-3 (iii).

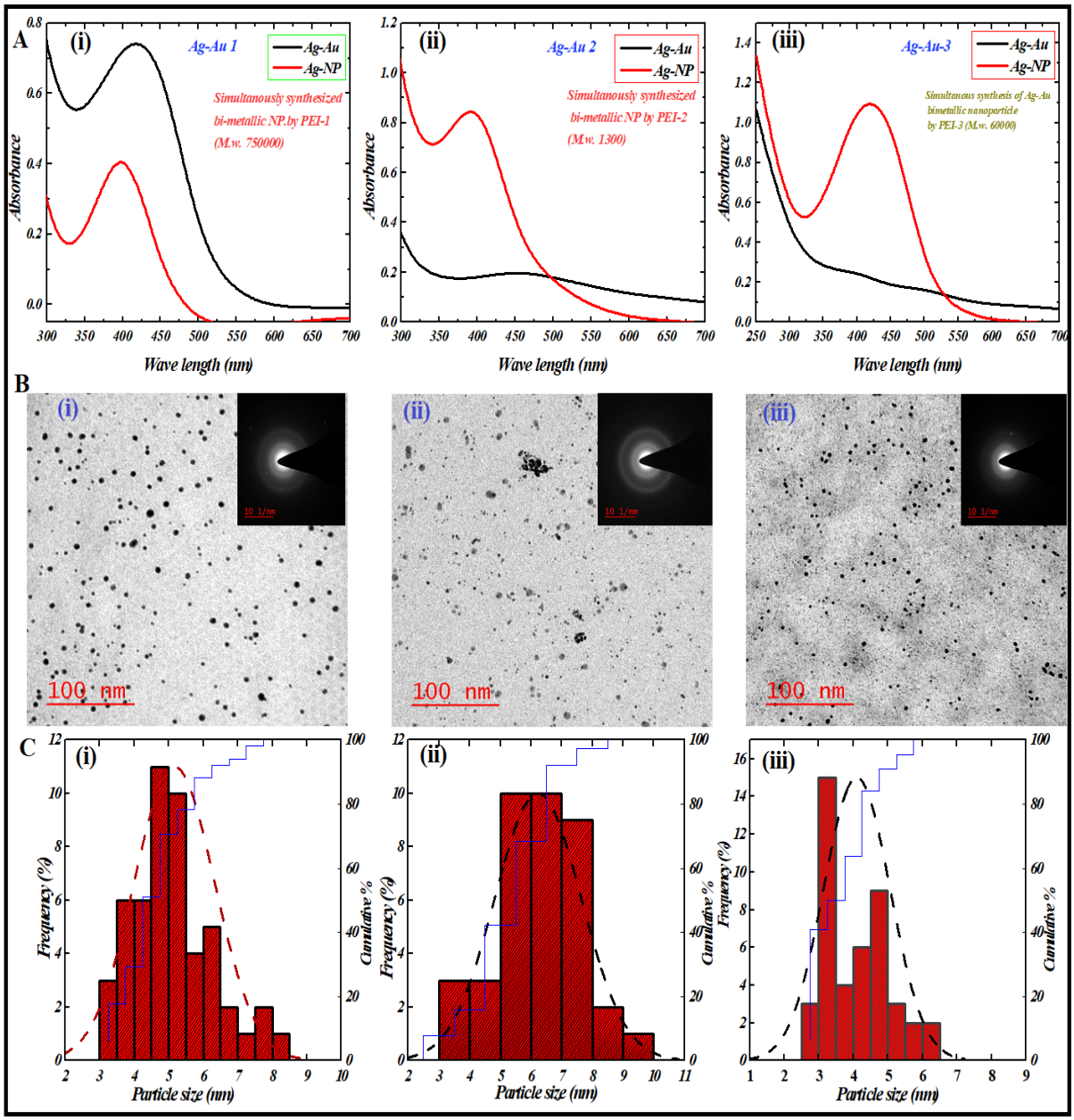

Figure 3.2 (A) Representing the characterization of synthesized AgNPs by UV-Vis Spectrophotometry, Ag-Au-1 (i), Ag-Au-2 (ii) and Ag-Au-3 (iii); (B) Showing the

characterization result of synthesized as Ag-Au by TEM imaging with their SAED pattern, and (C) size distribution plot; Ag-Au-1 (i), Ag-Au-2 (ii) and Ag-Au-3(iii).

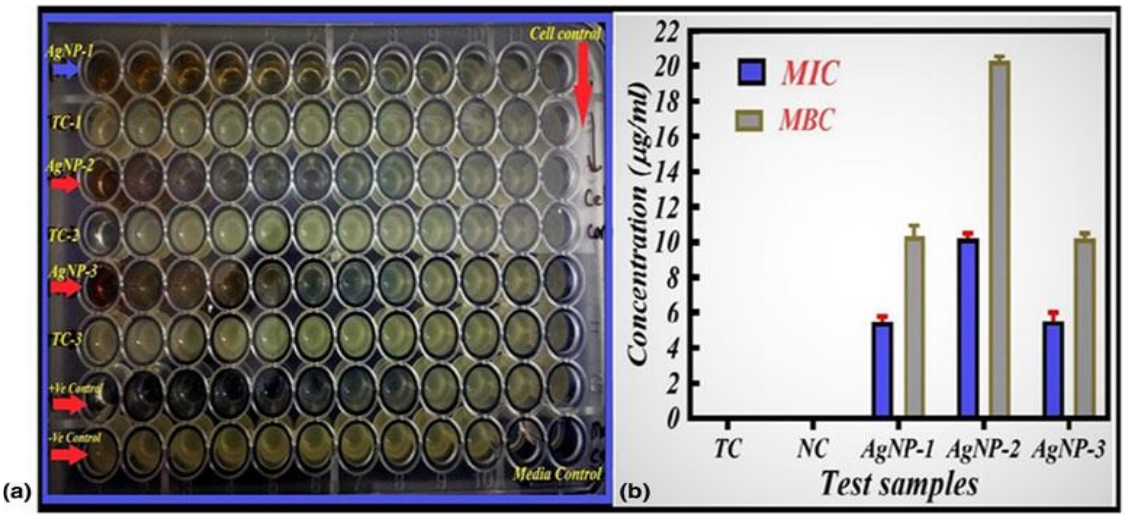

Figure 3.2- The antibacterial activity assessment microtiter plate (A); MIC and MBC (µg/ml) values of each Ag-NP against *A. baumannii* planktonic cells (B). TC represents Test control while NC is negative control.

3.3.3 Dynamic fluorescence quenching of fluorescein by PEI-capped Ag-NPs

It has previously been demonstrated that the bactericidal ability of AgNPs is potentiated by light. The photosensitization phenomenon was explored to understand the dynamic interaction between silver nanoparticles and proteins. To trigger light emission, we utilized fluorescein, which shows emission in the visible range. Silver nanoparticles showed good quenching of fluorescence, so fluorescence imaging was used to understand protein–nanoparticle interactions. In the present work, we have analyzed the quenching behavior of PEI-capped Ag-NPs in the presence and absence of *A. baumannii*; fluorescein was used as a fluorophore in these studies. It was observed that as-synthesized Ag-NPs quenched the intrinsic fluorescence of fluorescein molecules by nearly 60% [Figure 3.3(A) and 3.3(B)]. However, when cells (10^4 cells) were added to the media, the quenching percentage decreased significantly to 40% (with an associated increase in cell number). The quenching subsequently decreased to 10%. To understand the quenching dynamics of the AgNPs, 3D fluorescence spectra [Figure 3.3(C)]

were recorded; the results of these studies indicate that AgNPs show more affinity toward cell surface-expressed proteins than fluorescein molecules in a cell number-dependent manner. The mechanism of this dynamic quenching behavior of AgNPs is shown in Scheme 1.

3.3.4 Cell surface interaction and membrane breakage of *A. baumannii cells* by Ag-NPs

The 2D (Figure 3.4) and 3D (Figure 3.5) intrinsic fluorescence spectra of standard protein bovine serum albumin (BSA) and *A. baumannii* cells were recorded using EEM at 280/300 nm with control and after treatment with AgNPs with several MWs for 1 or 3 h. It was observed that in the control system, standard protein BSA and *A. baumannii* cells showed an intrinsic fluorescence

Emission on 330 nm (the peak associated with tryptophan); no other emission peak was observed. After treatment with PEI-capped Ag-NPs for 1 h, it was observed that AgNP-2 interacted very quickly with tryptophan residues of BSA and cell surface-expressed proteins; as a result, tyrosine residues (with a peak at 310 nm) were exposed, followed by denaturation of the quaternary structure of the protein. AgNP-1 and AgNP-3 showed similar interactions with BSA and cells; quenching in the intrinsic fluorescence of proteins up to 60% and partial denaturation were observed [Figure 3.4(a i, ii) and 3.5 (a)]. Furthermore, when the incubation time was increased to 3 h [Figure 3.4 (b i, ii)], the interaction dynamics with BSA were changed; AgNP-1, AgNP-2, and AgNP-3 showed denaturation of the quaternary structure of the protein, exposing tyrosine residues. Moreover, in the presence of *A. baumannii*, AgNP-1 and AgNP-3 showed more significant quenching in fluorescence; AgNP-2 completely denatured the surface proteins. To understand cell membrane damage, cells were incubated for 6 h with different AgNPs; centrifugation of the cell-containing solution was performed; fluorescence spectroscopy (EX/EM at 280/300 nm) of the supernatant was recorded as shown in Figure 3.6. It was found that all three AgNPs caused partial and complete denaturation of proteins, indicating cell membrane breakage.

The possible mechanism of membrane breakage is that AgNP-1 exhibits a larger size and a higher cationic activity than AgNP-2 and AgNP-3. In turn, AgNP-1 cannot pass the outer membrane and interfere with membrane potential, denaturing the surface-expressed proteins; this process generates reactive oxygen species, followed by an oxidative burst by the cell. AgNP-2 and AgNP-3 are smaller and have lower M_W; these particles can pass easily through the outer membrane via porins. They can enter the cell via channels and interact with both cytoplasmic and transmembrane proteins, resulting in the collapse of cellular physiology.

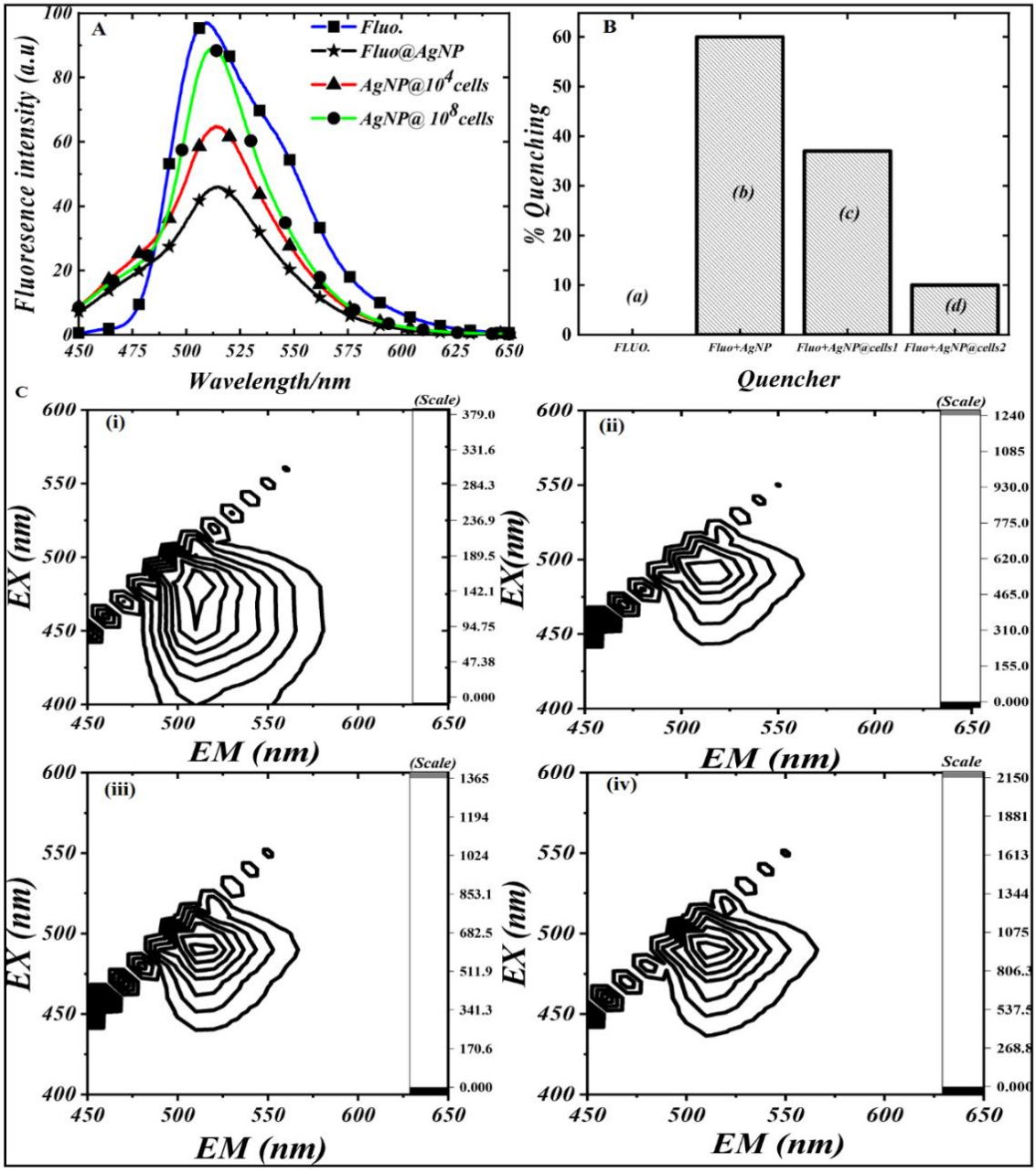

Figure 3.3 A- 2D fluorescence dynamic quenching analysis of fluorescein by PEI capped Ag-NP in the presence (iii & iv) and in the absence of *A. baumannii* cells (ii); while (i) showing fluorescein blank. (B)- Graph showing the quenching and de-quenching (%) of fluorescein by AgNPs in the presence (a); and in the absence of AgNPs (b); on addition of 10^4 cells/ml (c); and further increased 10^8 cells/ml (d). (C) 3D fluorescence imaging of dynamic quenching of fluorescein by AgNPs in the presence (iii & iv) and in the absence of *A. baumannii* cells (ii); with fluorescein blank (i).

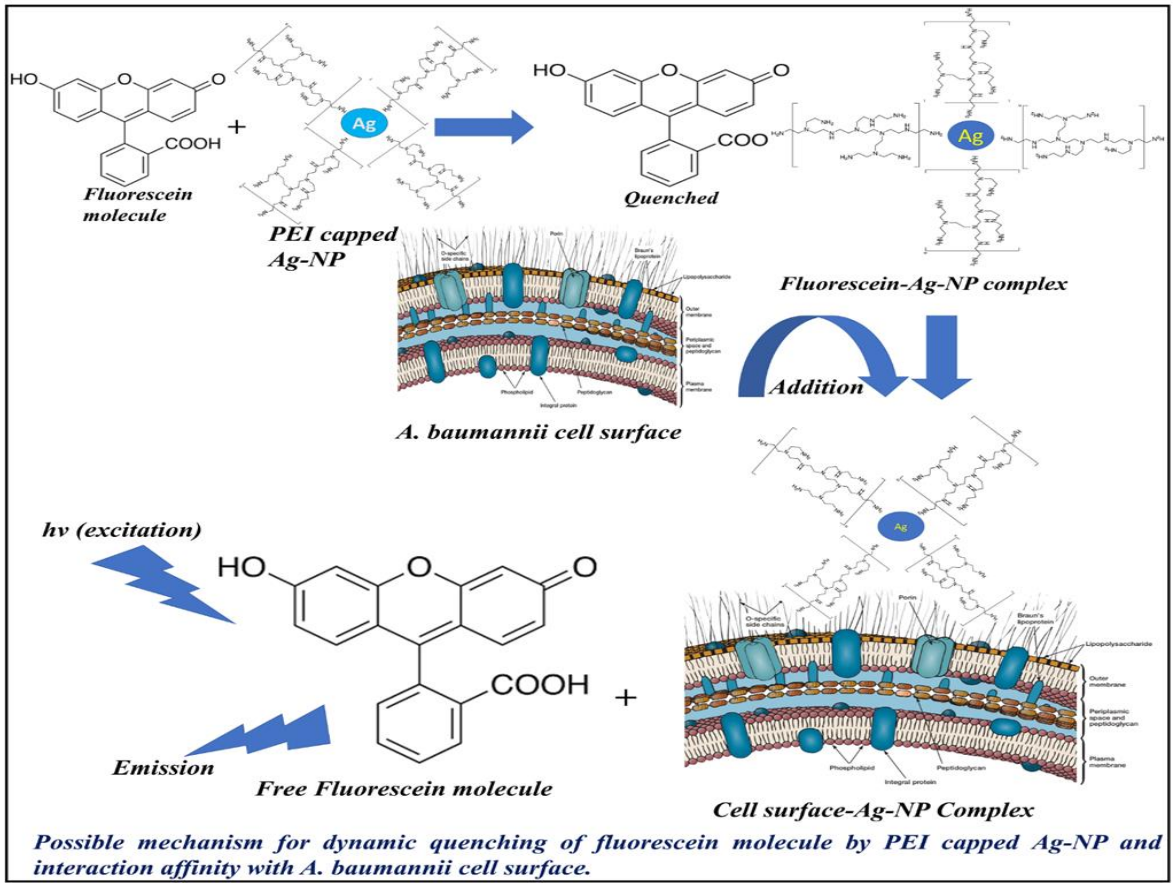

Scheme 3.2. Representing the possible mechanism of dynamic quenching behavior of PEI-capped AgNPs to fluorescein and interaction affinity towards *A. baumannii* cells.

Accordingly, polymeric M_W plays a central role not only in the synthesis of silver nanoparticles but also in the selective transfusion ability of AgNPs across the cytoplasmic wall. The AgNP-2 made with PEI exhibiting an M_W of ~1300 Da allows high efficiency of AgNP-2 transfusion

and selective interaction with cytoplasmic biomolecules (as evidenced by the fluorescence imaging, which revealed an additional fluorescence peak between 420 and 440 nm). The impact of the cationic polymeric weight on the selective movement of AgNP-2 and AgNP-3 across the cytoplasmic membrane, as described in this chapter, has not previously been described. The toxicity of silver nanoparticles is an important parameter that affects the clinical use of these materials; the findings on the stability of silver nanoparticles during antimicrobial action seem to be quite reasonable. The earlier finding demonstrated that AgNP affects the cell wall; it does not kill the cell. In addition, the study indicated that AgNP is not toxic to the *E. coli* K-12 strain, whereas silver ions showed potent toxicity under similar conditions. These previous studies directed the current evaluation of the AgNP function. Overall, in environmental assessments, considerations of the combined toxicity of dissimilar NPs will allow more accurate assessments of their environmental risks.

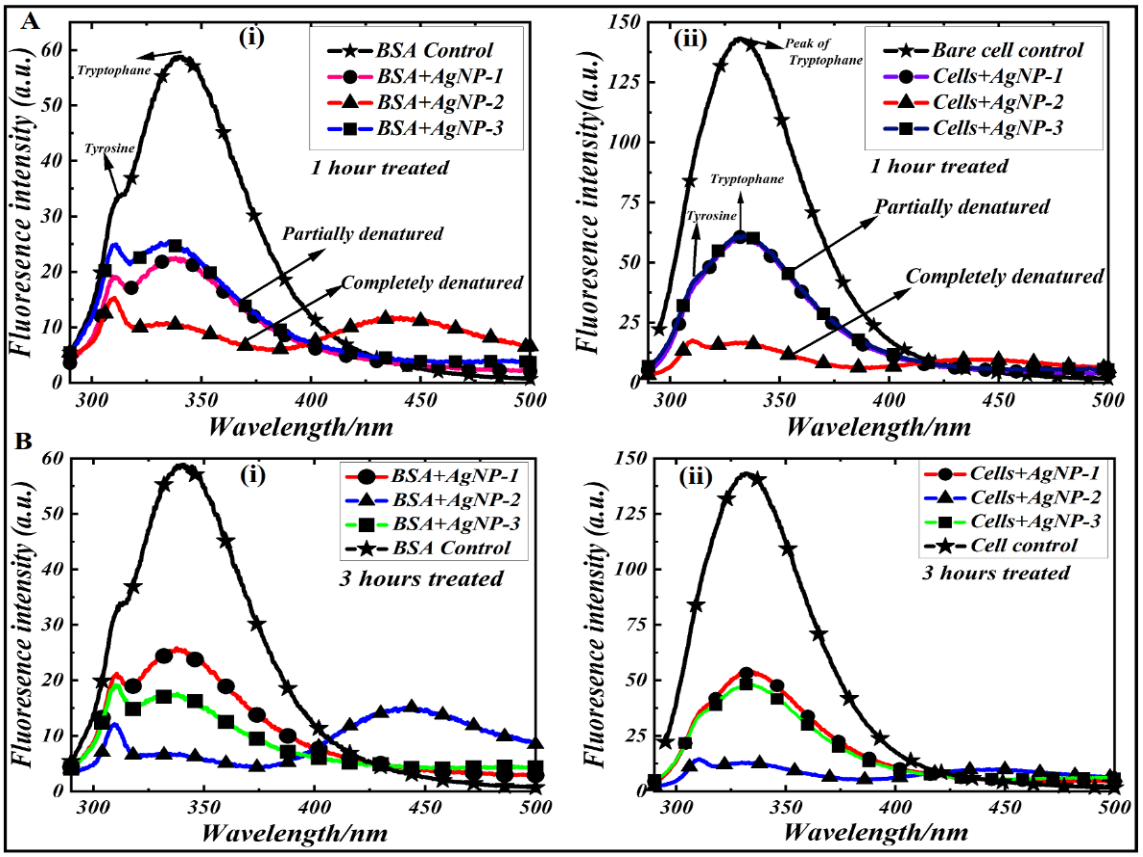

Figure 3.4 2D fluorescence spectra of *A. baumannii* and BSA, treated with synthesized AgNPs (1-3) for 1 and 3 hours. A (i) showing the spectra of BSA treated with AgNPs) for 1 hour; and cells treated similarly (ii); B (i) showing the of BSA treated with AgNPs for 3 hours, and cells treated similarly (ii).

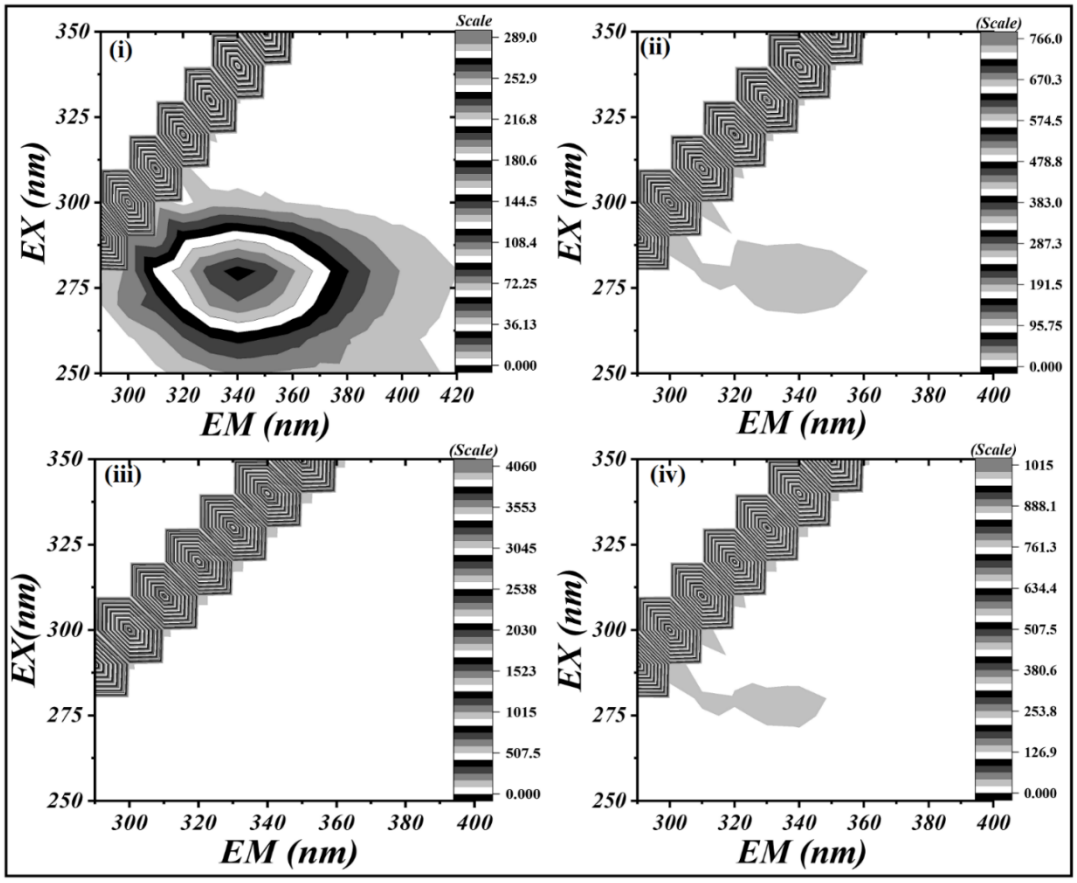

Figure 3.5 A shows the 3D fluorescence contour plot of BSA (5 µg/ml) (i); treated with AgNP-1 to 3 (5µg/ml) (ii-iv) for 1 hour at room temperature.

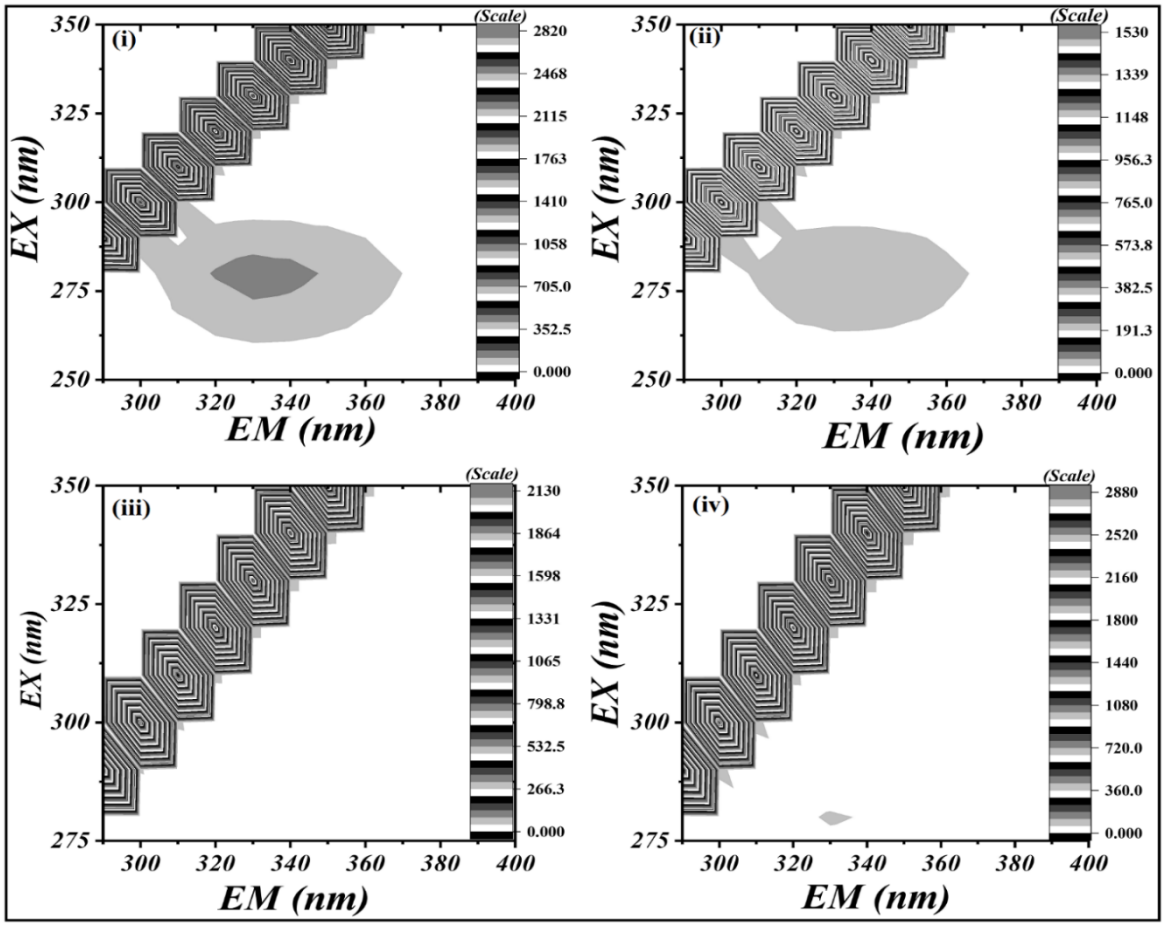

Figure 3.6 B. shows the 3D fluorescence contour plot of bare *A. baumannii* cells (10^6 cells/ml) (i); treated with AgNP-1 to 3 (5µg/ml) (ii-iv) for 1 hour at room temperature.

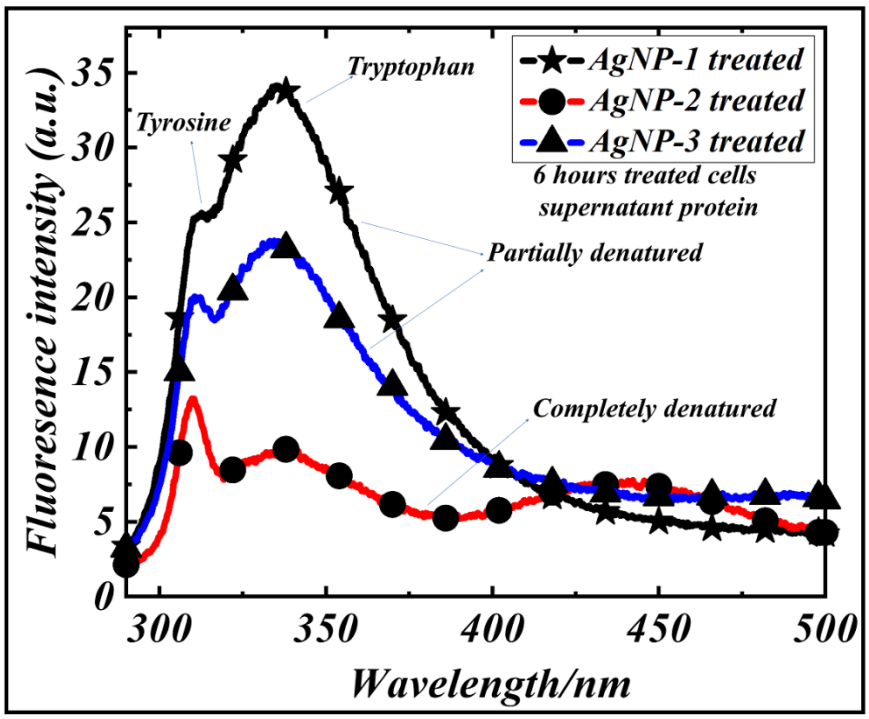

Figure 3.7 Representing the 2D Fluorescence spectra of supernatant of 6 hours treated cells with AgNPs (1-3).

3.4 Discussion

Cationic polymers, such as PEI, have intrinsic highly positive charges and have historically been employed in the materials for bioengineering. However, the demand for intelligent systems with high efficiency, bio-mimetic, and tuneable features is increasing. Artificial composites that mimic biorecognition and periodic structures may propel the development of advanced materials with outstanding properties. Polyethyleneimines (PEIs) constitute a valuable class of polycations because they have repetitive structural units, a wide molecular weight range, and flexible polymeric chains, which facilitate the customization of functional composites. Specific advantageous features could be introduced by purposeful modification or functionalization, such as specificity and sensitivity, distinct geometry, biocompatibility, and long service life. Thus, PEIs have been rapidly used in a wide range of applications in the fields of biomedicine, biotechnology, and biomaterials science. In the continuation, mono-metallic and bi-metallic nanoparticles (silver and gold) were synthesized in a rapid reaction system by using microwave irradiation that allowed homogenous heat distribution in the reaction mixture and controlled nucleation process. The synthesized monometallic silver nanoparticles have demonstrated excellent antimicrobial activity as coated with variable molecular weights of cationic PEI as discussed in the result section. Mechanistically, strong electrostatic forces in PEI molecules are responsible for the steric stabilization of silver ions in the micro-domains of the PEI. Accordingly, interestingly, different molecular weights and concentrations of PEI controlled the nano-geometry as well as the zeta potential of prepared AgNPs. Higher molecular weight PEIs such as 750 and 60kDa., allowed the formation of 20 and 3.0 nm of AgNPs respectively with highly positive zeta potential (+32 mV) suggesting a stable colloidal suspension of silver nanoparticles. However, when in a simultaneous reaction mixture, bi-

metallic Ag-Au is prepared the size of particles gets reduced to 5 nm. On the other hand, lower molecular weight (1.3 kDa) allowed the formation of an average of 5 nm size of AgNPs. Similarly, varying concentrations of these PEIs also controlled the LSPR of nanoparticles and all three AgNPs required a particular concentration of PEIs to attain characteristic SPR and control over the nano-geometry of AgNPs as attributed in Table 3.2.

Table 3.2 The influence of PEI concentration on the LSPR and absorbance intensity of as-prepared AgNPs.

PEI conc. (mg/mL)	**Conc. Of $AgNO_3$ (mM)**	**Conc. Of cyclohexanone/formaldehyde (µL/mL)**	**Absorbance maxima (nm)**	**Absorbance intensity (a.u.)**
		AgNP-1 (PEI mw. 750 kDa.)		
6.25	10	20	425	0.01
12.50	10	20	403	0.03
25.0	10	20	403	0.09
50	10	20	403	0.21
100	10	20	398	0.5
		AgNP-2 (PEI mw. 1.3 kDa.)		
6.25	10	10	402	1.4
12.50	10	10	403	0.7
25.0	10	10	403	0.1
50	10	10	na	Na
100	10	10	na	Na
		AgNP-3 (PEI mw. 60 kDa.)		
4.15	10	20	403	0.25

8.30	10	20	410	0.60
16.6	10	20	412	1.1
33.0	10	20	410	0.50
66.0	10	20	425	0.60

Further, PEI-coated AgNPs allowed selective transfusion of AgNPs across and interfered with membrane integrity by interacting with surface-expressed proteins, displaying variable antimicrobial efficiency as a function of molecular weight. High MW. of PEI-coated AgNPs (1 and 3) had a higher cationic surface charge that allowed strong interaction with the relatively negatively charged bacterial cell surface. This electrostatic interaction-induced cellular damage takes place either by pit hole formation (AgNP-1) while AgNP-2 and 3 can evade the cell barrier due to small size and destroyed internal structures by inducing reactive oxygen species. To reveal the affinity of AgNPs, towards bacterial surface-expressed proteins, an excellent experiment was performed. AgNPs can quench the fluorescence of fluorophore fluorescein by absorbing radiative energy at excitation. However, in the presence of bacterial cells, the quenching ratio was decreased gradually as a function of no. of bacterial cells as demonstrated in Figure 3.3, which confirmed the specific molecular interaction of AgNPs to the bacterial cell surface. The interaction of AgNPs with the cell surface (nano-bio interface) was dependent on the surface charge of nanoparticles. AgNP-1 and 3 had a strong affinity towards the cell surface in contrast to AgNP-2. Similarly, MIC and MBC values were lowest in the case of AgNP-1 and AgNP-3 as attributed in Figure 3.2. Due to the similar zeta potential of AgNP-1 and 3, the MIC and MBC values were the same as compared to AgNP-2. Further, it is revealed that zeta potential played a significant role in the antibacterial activity of AgNPs in addition to the size of nanoparticles.

From a cytotoxic point of view, in-vitro cell assessment studies have reported that AgNPs are toxic to several human cell lines including human bronchial epithelial cells, human umbilical vein endothelial cells, red blood cells, human peripheral blood mononuclear cells, immortal human keratinocytes, liver cells, etc. AgNPs induce a dose-, size, and time-dependent cytotoxicity, particularly for those with sizes ≤10 nm. Furthermore, AgNPs can cross the brain-blood barrier of mice through the circulation system based on in vivo animal tests. Ag-NPs tend to accumulate in mice organs such as the liver, spleen, kidney, and brain following intravenous, intraperitoneal, and intratracheal routes of administration. In this respect, AgNPs are considered a double-edged sword that can eliminate microorganisms but induce cytotoxicity in mammalian cells.

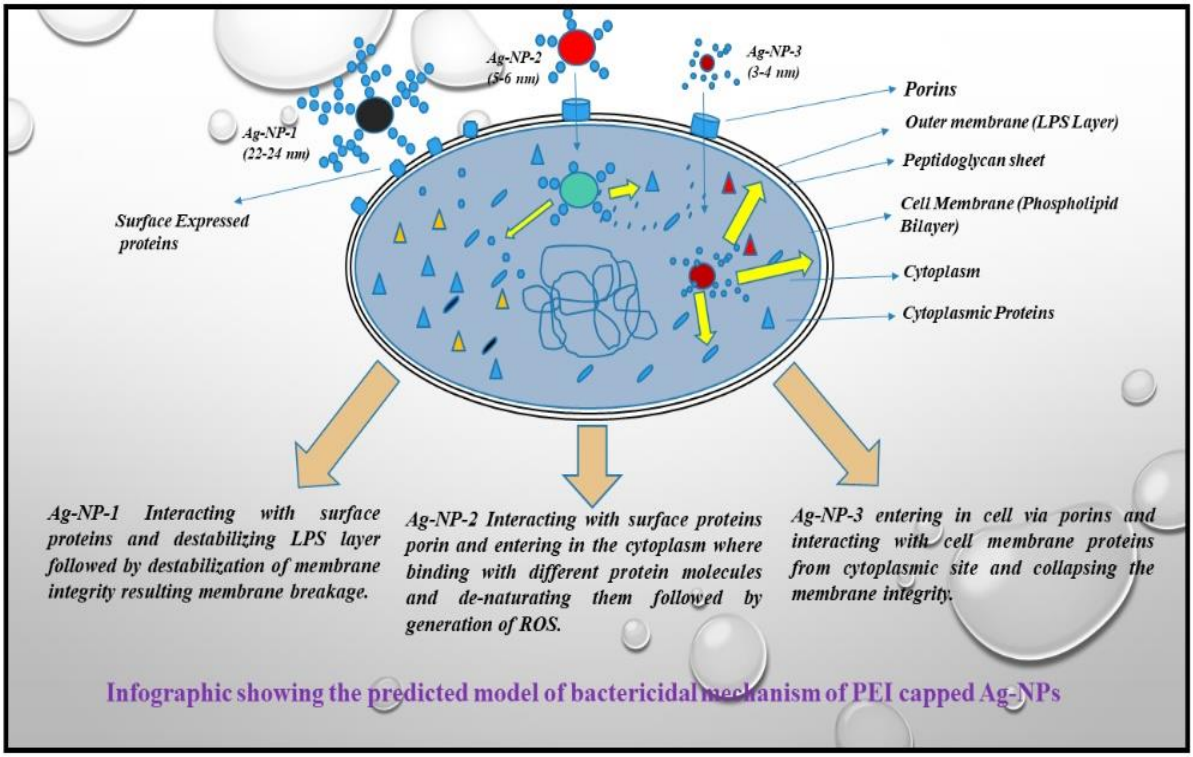

Scheme 3.3 Representing predicted model of the bactericidal mechanism of PEI-capped AgNPs.

3.5 Conclusion

Synthetic cationic polymer-mediated synthesis of silver nanoparticles and selective antimicrobial activity was demonstrated. Polyethyleneimine (PEI)-coated silver nanoparticles showed antimicrobial activity against *A. baumannii* as a function of PEI's polymeric molecular weight (M_W). Silver nanoparticles were coated with PEI of three different M_Ws: AgNP-1 with PEI exhibiting an M_W of 750,000, AgNP-2 with PEI exhibiting an M_W 1300, and AgNP-3 with PEI exhibiting an M_W of 60,000 kDa. These nanoparticles showed a particle size distribution of 4–20 nm. The nanoparticles exhibited potent antimicrobial activity against *A. baumannii*, with the minimum inhibitory concentration of AgNP-1, AgNP-2, and AgNP-3 about 5, 10, and 5 μg/mL, respectively, and minimum bactericidal concentration of AgNP-1, AgNP-2, and AgNP-3 on the order of 10, 20, and 10 μg/mL, respectively. Fluorescence spectroscopy of AgNPs revealed selective transfusion of AgNPs across the cell membrane as a function of the polymer M_W; differential interaction of the cytoplasmic proteins during antimicrobial activity was observed.